1 OF 1
AD
A103690

END
DATE
FILMED
10 81
DTIC

AD A103690

FOREIGN TECHNOLOGY DIVISION
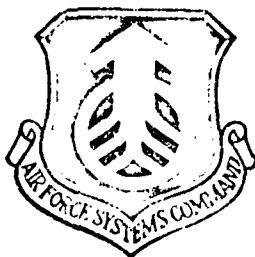
JOURNAL OF ENGINEERING THERMOPHYSICS

(Selected Articles)

DTIC
ELECTE
SEP 3 1981
S D

D

DTIC FILE COPY.

81 9 02 047

EDITED TRANSLATION

TABLE OF CONTENTS

EXPERIMENTAL RESEARCH ON THE CIRCULATION CONTROL
DESIGN METHOD FOR TURBINES*

Turbine Design Group, Zhuzhou Aircraft Engine Research Institute**
Turbine Testing Group, Shenyang Aircraft Engine Research Institute

ABSTRACT

A single-stage turbine is designed by utilizing the circulation control method [1]. This method has broken the conventional rules of design. A model experiment is conducted in order to verify the reliability of the method. General characteristics are measured over a wide range. The measurements of the efficiency distribution along the blade span and of the inlet- and exit velocity triangles of the rotor blades are made around the design point. The main test results are given in this paper and a simple analysis is made. The results indicate that the main characteristics istics of the circulation control design method are verified and the design requirements are satisfied. The method is practicable basically.

I. INTRODUCTION

The design of aircraft turbines has been conducted according to traditional equi-circulation, equal to α_1 or the mixed rules derived from them. The variation of the degree of reaction along the blade span is relatively large. Numerous experimental investigations have shown that the flow conditions at the root and the tip are not desirable. The second order loss and the leakage loss at the tip of the blade is relatively large. With the advancement

---

made in the study of the internal flow of turbines and in the application of computers, it is possible now for the designers to bypass the traditional design laws. Utilizing the complete radial equilibrium equation to control the distribution of the circulation $V_\theta R$ along the blade span, the degree of reaction at the root is raised while the degree of reaction at the tip is lowered. The flow conditions at both the root and the tip are improved and so is the performance of the turbine. In 1972 we established a research group to conduct work in this area. A computer program was developed in coordination with the computing laboratory at the Academy of Sciences and calculations were made. In May 1975, a single-stage turbine was designed. This is the first trial violating the conventional design method. Reference [1] describes the method of circulation control design and its main characteristics. The main results of the design are also presented. In order to verify the reliability of this new design method and to draw a conclusion, a test model was designed and a first stage testing is carried out on the model turbine tester in Shenyang from April to July, 1978. In this paper, the principal results of the test are presented and the fundamental analysis is made.

1. Test model

The prototype is a single-stage turbine. When designing, the complete radial equilibrium equation is employed at the gaps in the axial direction to control the distribution of the circulation $V_\theta R$ along the blade span, intending to improve the flow conditions at the root and the tip. The work along the blade span is linearly distributed on the whole. The variation of the work is 7.56%. Uniform velocity coefficient distribution is taken along the blade span, that is, for the guiding blade, $\phi = 0.96$ and for the rotor blade, $\psi = 0.95$. The design load is relatively high. The main parameters are: effective work $L_T = 21,770$ kg-m/kg, loading coefficient at the midspan is $\mu = 2.085$, stagnation expansion ratio π_T^* = 2.39, design efficiency $\eta_T^* = 0.879$. The Mach number at the exit

2

of the guiding blades is relatively high and the flow is found to be supersonic near the root region. At the root $M_{c1} = 1.114$. The scale of the test model is m = 0.75. The flow channels, the main measuring positions and parameters are shown in Figure 1.

The relative measurement error of the stagnation efficiency, the relative net flow rate, and the net work at the large expansion ratio condition is around ± 1.0%.

The rotor blades are capped and at the cold condition, the radial gap at the blade tip is 0.5-0.8 mm, which is 0.8-1.27% of the blade span.
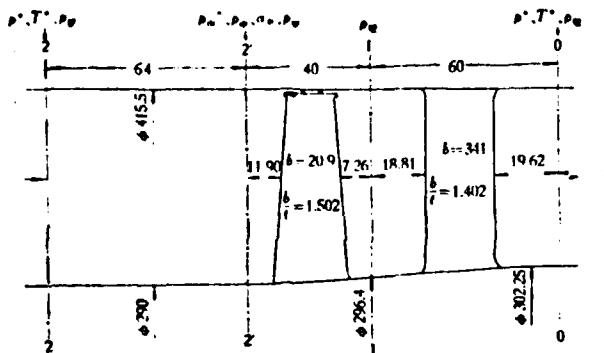
Figure 1. The flow channel and the measuring positions

2. Test results and analysis

(a) Performance at the design point

The tested values and the designed values of the main performance parameters are compared below:

(b) Stagnation efficiency

Based on the average value of the multiple points total pressure at section 2-2 far downstream and the torque of the hydraulic work detector, the stagnation efficiency η_{TO-2}^{*} of the single-stage

	Stagnation efficiency		net effective work $\overline{L}_e$	relative net flow rate $\overline{G}$	throat area of the guiding blade A_t (cm)^2
	measured value at far down-stream n^*_{TO-2}	measured value at near down-stream $n^*_{TO-2'}$			
tested value	0.884	0.909	20.0	0.99	229
designed value	0.879		20.16	1.0	232.8
relative deviation	0.57%	3.41%		1%	-1.65%

turbine is calculated. The efficiency at the design point meets the original design requirement.

It should be pointed out that the efficiency calculated by the single-point total pressure at near downstream is 1.5-4% higher than that calculated by the multiple points total pressure at far downstream. The deviation of the expansion ratio is relatively larger, which is 2.8% higher than that at the design point. After analyzing, it is more desirable to take the far downstream results. The static probe behind the rotor blade detects a pulsive flow with a frequency of about 10,000 Hz. When the tangential velocity is larger than the absolute velocity of the flow, the pressure detected is higher than the true value. The existence of a vortex flow behind the rotor blade leads to a loss in the total pressure. The loss cannot be measured accurately at the near downstream since the probe suffers the "choking effect" if it is placed close to the trailing edge. Hence, in order to make accurate measurements, there should be a straight section behind the rotor blade. The fixed probe should be placed at the nearly uniform region of the flow. For the transonic turbine, this region is two or three cascade widths behind the cascade [2]. At the point 122.8 mm away from the trailing edge of the guiding blade, there is still a wave motion of 37 mm Hg column (Figure 2). This wave is induced by the wake of the guiding blade passing through the rotor blade. This phenomenon indicates

that the wake of the transonic cascade is relatively long and
that it is more desirable to calculate the total pressure by the
static pressure at the exit and other measured parameters [3].
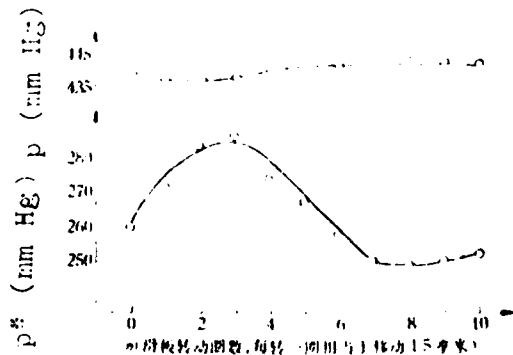
n(No. of revolutions of slide plate, each revolution corresponds
to a movement of 1.5 mm).
Fig. 2. The variations of the total pressure and the static
pressure along the cascade width far downstream of the rotor blade.
(conditions are maintained with an error of ˉ4 mm Hg).

(c) The relative net flow rate

It is evident from the tested characteristics that the throat
of the guiding blade at the design point is the critical cross-
sectional area. The guiding blade throat area of the test model
is 1.65% smaller than the designed value, causing the net flow
rate to be slightly less than the designed value.

II. INTERNAL FLOW PATTERN OF THE TURBINE NEAR THE DESIGN POINT

In order to study the internal flow pattern in the turbine of
circulation control design, measurements along the blade span are
made near the design point ($\bar{n} = 1.0$, $\pi_T^* = 2.3$). Measurements are
made with the combination probe for the total pressure, the direc-
tion, the static pressure and total temperature at the nine radial
positions along the 45° line 19.5 mm from the guiding blade and
76 mm from the rotor blade. It is also moved along the cascade
width behind the guiding blade. The results are tabulated through
a wire-expansion type transducer and recorded continuously by an

automatic six point recorder. The mean value is calculated according to the area integral. For the region where m > 1, the total pressure and the linearly distributed values of the static pressure on the inner and outer walls detected by the probe are corrected according to the normal shock relations.

1. Flow parameters at the exit of the guiding blade

One essential characteristic of the circulation control design is the "reverse twist" of the exit angle of the guiding blade, that is, the angle is greater at the root and smaller at the tip. The measured value along the blade span is relatively smooth and is almost parallel to arcsin(a/t) of the guiding blade except at both ends. If a translation is made, it is observed that they are identical for most of the region. The deviation is due to systematic error. The measured values and the trend of the exit angle α_{1k} do not agree. Calculation utilizing the measured values indicated that the β_1 at the root is larger than the designed value. These results are shown in Figure 3.

A linear distribution of static pressure between the inner and outer walls is taken at the exit of the guiding blade. The exit total pressure and the exit velocity coefficient along the blade span are almost constant for most part of the region except at the two ends, where they are slightly smaller (Figure 3, Figure 5). This indicates that the second order loss of the guiding blade is not large at all and the region affected is relatively small. The mean value of the velocity coefficient φ_{0-1} = 0.9815 is higher than the designed value 0.96. This is because the measurements made do not detect the loss completely. The flow afterwards will still be undergoing a mixing process.

Another characteristic of the circulation control design is the gradual increase of the slope and the curvature of the streamlines. The streamlines are squeezed against the root. This is

proved by the relatively large value of M_{c1a} calculated from the measured results. This also justifies the necessity of considering the slope and curvature of the streamlines in the circulation control design (Figure 3).
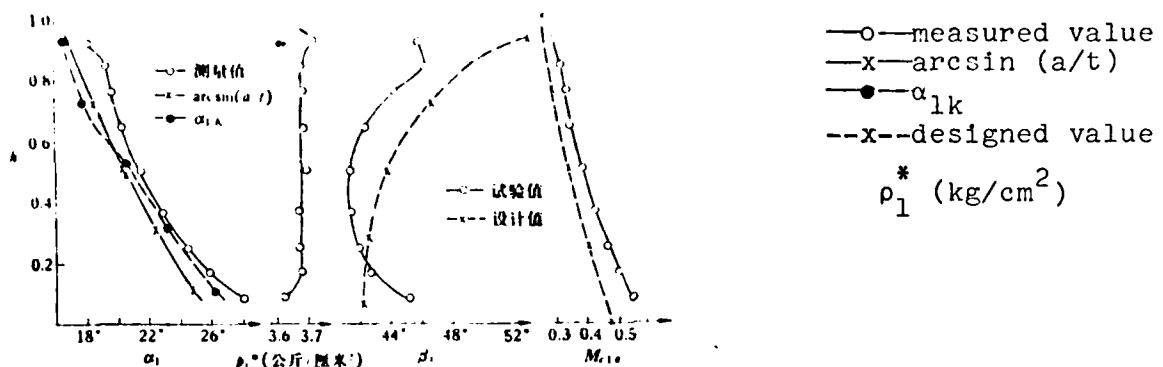

Figure 3. The distribution of the exit parameters of the guiding blade along the blade span.

2. Flow parameters at the exit of the rotor blade

Measurements along the blade span are made at the far downstream section 2-2. The measurement for the absolute flow angle at the exit is repeated twice and is found to be consistent. There is a slight deviation in the lower half region but its value is closer to the designed value. Within the region $\frac{1}{3}$ blade height from the tip, the deviation is larger (up to 20°) due to the leakage loss effect. Comparison between the relative flow angle and the arcsin (a/t) of the rotor blade shows a similar situation. The deviation at the tip is approximately 5°. (Figure 4).

The exit total pressure is relatively low at the mid span and is relatively high at the 30% and 80% blade height. It falls sharply at both ends, producing a saddle shape. The exit static pressure is almost linearly distributed along the blade height (Figure 4). The off-design does not cause any large non-uniformity of the exit parameters.

$$\rho_2^* \ (\text{kg/cm}^2) \quad \rho_2(\text{kg/cm}^2) \quad \alpha_2(\text{deg}) \quad \beta_2(\text{deg})$$
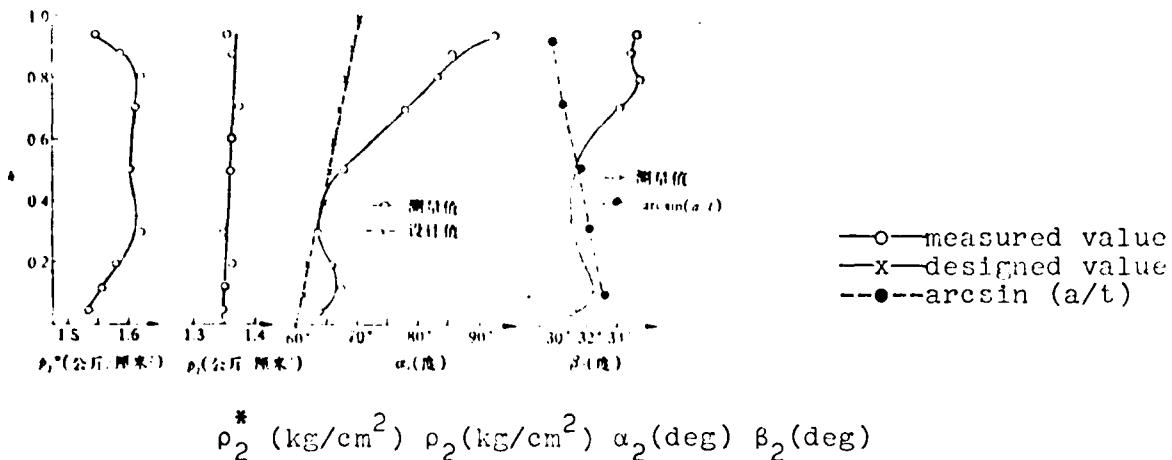
Figure 4. Distribution of the measured parameters far downstream of the rotor blade along the blade span

With the inlet and exit parameters obtained, the rotor blade velocity coefficient ψ_{1-2} is calculated, which reaches 0.97 in the mainstream region. It falls sharply at both ends since the intensity and the affected region are both increased with respect to that of the guiding blade due to the secondary flow effect (Figure 5). Its mean value is approximately 0.91, which is much lower than the designed value 0.95. This velocity coefficient is obtained from the measured parameters far downstream. The mixing loss at 76 mm behind the rotor blade is considered, and hence the measurement of the loss is more complete. Since the wake from the guiding blade is comparatively long, it is still under a mixing process when it reaches the rotor blade and even behind the rotor blade. This causes an undesirable operating environment for the rotor blade. Hence, part of the loss detected is induced by the guiding blade. During the design process, this kind of practical situation should be dealt with.

3. Stagnation efficiency

Based on the total temperature and the total pressure at the inlet and exit, the stagnation efficiency η_T^* is computed. At the 75% blade height, the efficiency reaches a maximum of 0.95. Within the region 30% blade height from the root, the decrease of the
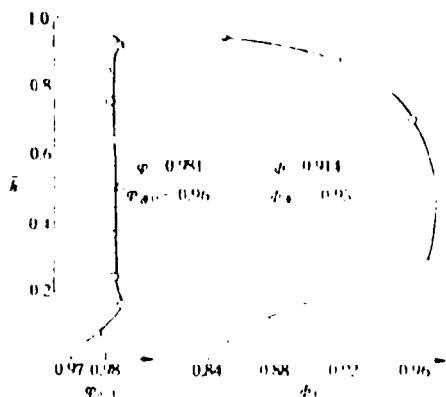
Figure 5. The distribution of velocity coefficient of the guiding blade ψ and the velocity coefficient of the rotor blade ψ along the blade span.

Figure 6. Variation of the stagnation efficiency along the blade span.

—o—experimental value
($\bar{n}$ = 1.0, π_T^* = 2.301)

———designed value
($\bar{n}$ = 1.0, π_T^* = 2.39)

efficiency is large. It also falls within the region 20% blade height from the tip (Figure 6). Employing the variation design, the function of the tangential velocity is enhanced and a favorable effect on the efficiency is produced.

From the results and discussion presented above, the main characteristics of the control circulation design are verified and the original design requirements are satisfied on the whole. The secondary flow behind the guiding blade is not so destructive. However, the effect due to the secondary flow behind the rotor blade and the leakage loss at the tip is quite significant. This causes a relatively large deviation of the flow parameters from the designed values at both ends, especially the deviation of the absolute exit flow angle at the blade tip (20°). Further consideration on the variable loss design should be made. This does not only require the second order leakage loss model at the tip, but also the model concerning the effect of the exit flow angle. Further studies on all these models are required.
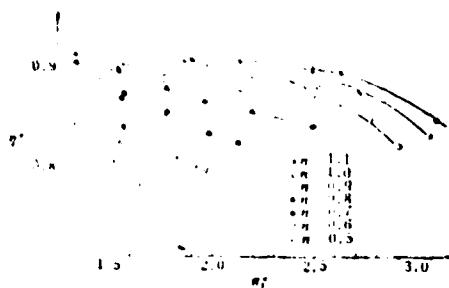
Figure 7. The stagnation efficiency vs π_T^* and $\bar{n}$

III. TEST FOR GENERAL CHARACTERISTICS

For the stagnation expansion ratio $\pi_T^* = 1.3$–3.08, and the converted speed of rotation $\bar{n} = 0.5$–1.1, the general characteristics are tabulated (Figure 7, Figure 8, Figure 9). How these characteristic lines vary from the general rules is not important and will not be discussed in detail here. However, the following problems should be discussed:
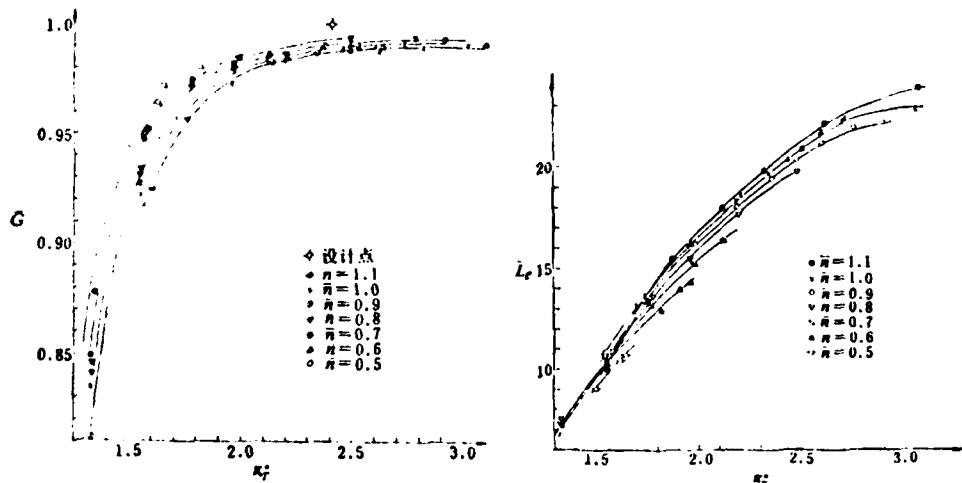
Figure 8. The relative net flow rate $\bar{G}$ vs π_T^*
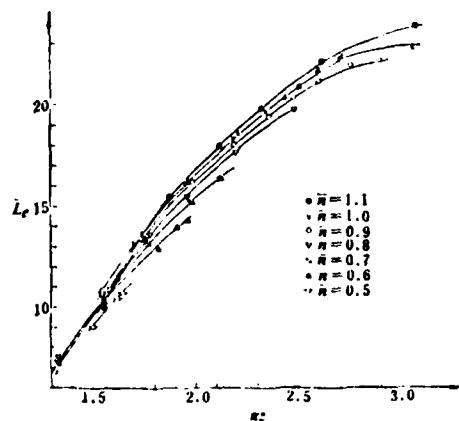
Figure 9. The net effective work $\bar{L}_e$ vs π_T^*

1. <u>The internal operating condition of the turbine under different states</u>

The internal operating condition of the turbine at the off-design condition can be observed clearly from the variation of the guiding blade expansion ratio p_0^*/p_1, the rotor blade expansion ratio p_1/p_2' and the stagnation expansion ratio p_0^*/p_2' vs the state (Figure 10). The corresponding curve of the degree of reaction is also shown (Figure 11). Degree of reaction $\rho_T = \dfrac{(p_0^*/p_1)^{-(k-1)/k} - (p_2^*/p_1)^{-(k-1)/k}}{1 - (p_0^*/p_2')^{-(k-1)/k}}$. With the increase of π_T^*, the guiding blade expansion increases linearly. Over-expansion appears at the root, causing a pressure diffusion condition ($p_1/p_2' < 1$, $\rho_T < 0$) at the root of the rotor blade. The root of the guiding blade reaches the critical condition quickly and the inclined plane exit expansion appears right afterwards. As the blade reaches the critical condition, the pressure perturbation behind it cannot be transmitted upstream. This prevents the inclined plane exit expansion at the root of the guiding blade from reaching the limit. Since the tip of the guiding blade does not reach the critical point, the pressure there will no longer increase. However, the inclined plane exit can still be expanding until its limit expansion ratio is reached. Hence the total expansion ratio increases continuously and the corresponding degree of reaction increases linearly. From the trend of the expansion ratio curve, it can also be seen that the circulation control design makes the flow in the radial direction to become more gradual. This does not only favor the design states, but also improve the non-designed states, especially the performance of the total expansion ratio. The variations of the expansion ratio and the degree of reaction with the speed of rotation are more or less similar.

2. The oscillation of the stagnation efficiency at the transonic region

Oscillation of the efficiency curve appears near the design point. A relatively greater number of measuring points is taken here and measurements are repeated once. These readings are found to be consistent, indicating that it is not simply an accidental phenomenon. The reasons are analyzed below: When designing the expansion ratio of the turbine, the operating condition of the

guiding blade is unchanged basically, and so is the corresponding
angle of attack of the rotor blade. The exit Mach number of the
rotor blade is in the range 0.8-1.0. Hence, shockwaves are liable
to occur at the throat and the trailing edge. The shockwaves from
the trailing edge extend to the neighboring blade and cause separa-
tion of the boundary layer. When π_T^* increases the shockwaves lean
back and the separation point moves back. As the blade profile
becomes slender and the second order loss decreases, π_T^* further
increases. The intensity of the shockwaves increases and hence the
loss increases, producing an oscillating phenomenon. This pheno-
menon is common for plane cascade and ring cascade.
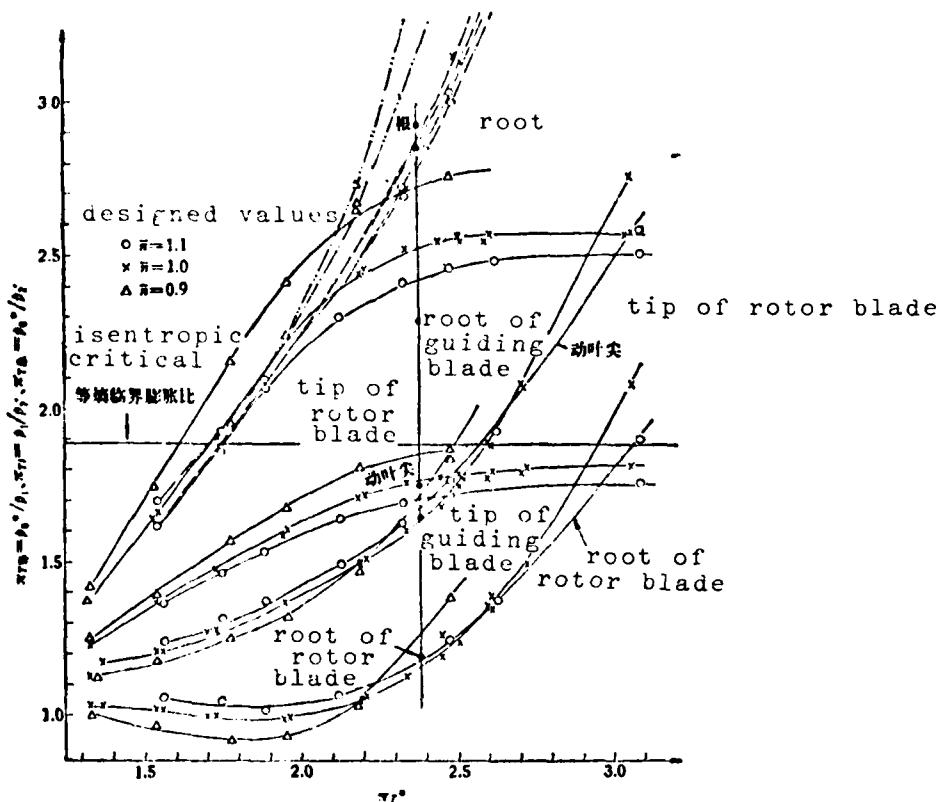
Figure 10. The variation of the expansion ratio vs state

Figure 11.   Variation curve of the thermodynamic degree of
reaction vs state

3. Transonic design is an effective way to increase the
stage load

From the curves of the stagnation efficiency and the net work,
it can be observed that the decrease of the efficiency curve is
not very sharp at relatively high π_T^*. But there is still a large
growth of the stage load. The related parameters are listed in
the table below:

π_T^*	2.4	2.6	2.7	2.8	2.85	2.9	3.0
η_T^*	0.884	0.883	0.876	0.864	0.86	0.852	0.84
L_e	20	21.5	22.1	22.5	22.6	22.7	22.8
$\Delta\eta_T^*/\eta_{Td}^*\%$	0	-0.113	-0.905	-2.26	-2.71	-3.5	-4.86
$\Delta L_e/L_{ed}\%$	0	7.5	10.5	12.5	13	13.5	14

The variation of the efficiency for π_T^* in the range 2.4-2.7
is relatively small, while the net work increases almost linearly.
The efficiency curve decreases linearly afterwards'. The increase
of the net work gradually decelerates since expansion ratio tends
to reach its limit. As the expansion ratio increases to 2.7, the
efficiency falls only 0.905% while the net work increases by 10%.
At this point, the relative exit Mach number at the mid span is
estimated as 1.05. The main factor affecting the efficiency in this

13

region is the exit Mach number. Hence the transonic design is a prospective way of increasing the stage load without greatly reducing the efficiency. Progress in this area can be expected through certain solid theories and experimental work.

IV. SUMMARY

The following can be concluded from the above analysis:

1. The turbine is designed by the circulation control method. The principal performance parameters at the design point satisfy the design requirement basically. The measurements along the blade span near the design point show that the principal characteristics of the circulation control design method are verified. Hence the method is applicable basically.

2. The secondary flow behind the guiding blade is not too essential while the intensity of the secondary loss behind the rotor blade and the region affected increases. Due to the leakage at the blade tip, the exit flow angle at the tip deviates greatly from the design value. Hence, further consideration of variation loss design is necessary.

3. The expansion ratio curve tabulated by means of the static pressure at the wall is very favorable to the understanding of the flow process inside the turbine. The analysis shows that the circulation control design does not only raise the performance of the design state, but also improves the performance of the non-design states, especially the total expansion ratio.

4. As the expansion ratio increases from 2.4 at the design point to 2.7, the efficiency decreases by approximately 1%, while the effective work increases by approximately 10%. This indicates that the transonic stage design for relatively high exit Mach number is a very prospective way to increase the stage load without

14

reducing the efficiency significantly.

5. The efficiency measured at the near downstream region of the rotor blade at the design point is 2.8% higher than that measured at the far downstream region. Hence, the section where measurements are made should be placed at the far downstream of the rotor blade exit, where the flow is more uniform.

REFERENCES

[1] 株洲航空发动机研究所涡轮设计组，航空涡轮控制环量设计，叶轮机械气动热力计算、设计与试验经验交流会文集，1976 年.
[2] T. B. Meger: *ASME paper*, 72—GT—43.
[3] S. F. Smith 等：涡轮和压气机的模型试验，现代航空发动机试验，中译本，第 199 页，国防工业出版社，1976 年 1 月.

THE EXPERIMENT RESEARCH ON THE TURBINE DESIGN OF CIRCULATION CONTROL METHOD

Group for Turbine Design in Designing Department of Zhuzhou Aircraft
Engine Factory, Group for Turbine Test of
Shenyang Aircraft Engine Institute

Abstract

A single-stage turbine is designed by using a circulation control method. It has broken the conventional law of design. A model experiment was conducted in order to demonstrate the reliability of this method. A general characteristic was measured over a wid range. The efficiency distribution along blade span and the inlet and outlet velocity triangle measurement of rotor blades were made around the designing point. The main test results are given and the simple analysis is applied to it. The results indicated that the main characteristics of the circulation control design got demonstration and the design requirement has been reached on the whole. This method is practicable.

THE CALCULATION OF TRANSONIC TURBINES
AT OFF-DESIGN CONDITION

Ge Man-Chu

Institute of Engineering Thermophysics, Academia Sinica

Abstract

A group of simultaneous equations, including S_2 stream surface equations, simplified S_1 stream surface equations (for solving the triangular region at the tail of the cascade), flow loss correlation and deviation angle correlation are obtained for the calculation of the direct problem of turbomachinery. By the solution of these equations, the design point as well as the off-design performances can be calculated.

The essential difference in treating subcritical, critical, and supercritical flow condition is considered. The influence of losses is taken into account in the calculation of choking conditions. A unified approach is adopted to solve these equations. Losses, deviation angles, and other flow parameters are obtained in the same iterative process, so that false choking conditions will not occur and convergence will be rapid. The computer program is then completed and may be used in the calculation of the off-design performance of transonic turbines.

Satisfactory results are obtained when applying this program to calculate the exit performance of the turbine stage. The reduced flow rate, the efficiency and the expansion ratio are fairly consistent with the experimental results. The difference between the calculated results and the experimental data is within 1%.

I. INTRODUCTION

In this paper, the S_2 stream surface equations of the 3-D flow theory of turbomachinery, the simplified S_1 surface of revolution equations (for the triangular region at the tail of

the cascade), the loss correlation equation and the equation
for the flow angle at the exit of the cascade are applied
simultaneously to solve the direct problem of turbomachinery.

The calculations of the losses and the exit flow angle
under different operating conditions are made with this set
of simultaneous equations. Hence not only the flow parameters
and the performance at the design point can be calculated,
but the flow parameters and performance at off-design conditions
may also be calculated.

The different characteristics of subcritical, critical,
and supercritical flow are taken into account during the cal-
culation process. Corresponding consideration of the losses
and exit flow angle is also made. At the same time, the influ-
ence of the losses on the calculation of the choking condition
is also considered. Hence a more reasonable result for the
choking flow rate can be obtained readily. For the calculation
of the losses and the exit flow angle, a unified approach to
the set of simultaneous equations is applied to obtain the
losses, flow angle, and other flow parameters at the same time.
This approach prevents the occurrence of the false choking
condition which is due to the iteration process for the losses
and the exit angle. These parameters are found to be in good
synchronism during the calculation. This is favorable to the
convergence of the solution of the set of simultaneous equa-
tions, and the convergence speed is greatly accelerated.

A computer program for calculating the transonic turbine
at off-design conditions is developed and is executed on the
TQ-16 machine. For a single stage turbine, the computation
time for each point is around 20 seconds. Calculations are
made for certain domestic as well as foreign-designed turbines.
For instance, off-design calculation is conducted for the 250
kw gas engine turbine designed and tested by the Institute of

17

Mechanics, Academia Sinica, and fairly satisfactory results are obtained. For the entire test range, the calculated values of the reduced flow rate, efficiency and expansion ratio are found to be consistent with the experimental data. The error is only about 1%. A trial calculation is also conducted for the turbine of the JT3D-3B engine, and it is found that the deviation of the calculated values of the three parameters from the given design-point data is also around 1%.

II. CALCULATION OF TRANSONIC OFF-DESIGN CONDITION

To meet the development of both defense and civil industries, the performance of the turbine at off-design conditions is gradually considered as a design parameter also. The two-element method is gradually employed to calculate the performance of the turbine at off-design conditions. But there is a deficiency in the calculation of losses, exit flow angle, choking, critical and supercritical flow conditions. In this paper, a further improvement of the method is attempted.

1. Assumptions, basic equations, and boundary conditions.
Assumptions: perfect gas, absolutely steady, or relatively steady insulated from the surrounding.
Basic equations (in relative coordinate system):

Continuity equation $\qquad \nabla \cdot (\rho W) = 0$

Momentum equation $\qquad -\nabla p/\rho = dW/dt - \omega^2 r + 2\omega \times W$

Energy equation $\qquad dI = 0$

Equation of state $\qquad p = \rho RT$

Thermodynamic relation $\qquad Tds = dh - dp/\rho$

18

Expression for loss $\Delta s = \dot{R} \ln \{1 + (Y_p + Y_s + Y_k)[1 - (1 + (\kappa - 1)M_1^2/2)^{\frac{1}{1-\kappa}}]\}$

Expression for exit flow angles $\beta_2 = \alpha_2 - \sum_{i=1}^{3} C_i M_i^{-1} + 4t/c$

This set of simultaneous equations can be used to solve the flow parameters at the subcritical conditions. The critical and supercritical cases will be discussed later.

The boundary conditions include the dimensions of the flow channel, the blade angle at the exit of the blade, the stagnation pressure and stagnation temperature of the flow at the inlet, the flow rate at the inlet or the back pressure at the exit. To solve for the losses, some characteristic dimensions of the blade must also be given.
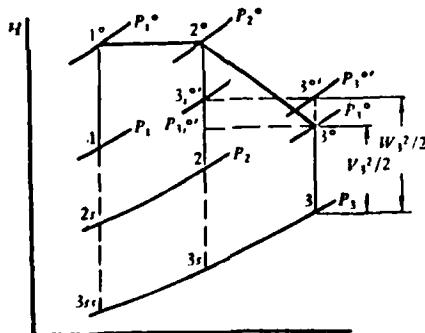

Figure 1. The enthalpy-entropy relation of the turbine stage.

2. The losses and the exit flow angle

The coefficients of pressure loss are

$$Y_N = (p_1^0 - p_2^0)/(p_2^0 - p_2) \quad Y_R = (p_2^{0'} - p_3^{0'})/(p_3^{0'} - p_3).$$

The relations among the parameters are shown in Figure 1.

The coefficients of stagnation pressure loss can be
expressed by the following equations:

$$\sigma_N = 1/\{1 + Y_N[1 - (1 + (\kappa - 1)M_1^2/2)^{\frac{\kappa}{1-\kappa}}]\}$$

$$\sigma_R = 1/\{(1 + Y_R[1 - (1 + (\kappa - 1)M_1^2/2)^{\frac{\kappa}{1-\kappa}}]\}$$

The stagnation efficiency of the turbine

$$\eta_T = (H_3 - H_1)/(\sigma_R^{\frac{\kappa-1}{\kappa}} H_3 - H_1)$$

The subcritical and supercritical cases should be consid-
ered separately for the calculation of losses. For the sub-
critical condition, the losses of the flow past the blades can
be classified into the profile loss, secondary flow loss, and
leakage loss. The following expressions can be applied for
common blade profiles:

Profile loss

$$Y_p = -\left(\sum_{j=1}^{3} A_j i_n^{j-1}\right)[Y_{p(\alpha=0)} + (\alpha_1/\beta_2)^2(Y_{p(\beta_1=\beta_2)} - Y_{p(\alpha_1=0)})](5C_{max}/b)^{-\alpha_1/\beta_2}$$

$$(\text{ when } \quad i_n < -3°)$$

$$Y_p = \left(1 + \sum_{j=1}^{3} B_j i_n^j\right)[Y_{p(\alpha=0)} + (\alpha_1/\beta_2)^2(Y_{p(\beta_1=\beta_2)} - Y_{p(\alpha_1=0)})](5C_{max}/b)^{-\alpha_1/\beta_2}$$

$$(\text{ when } \quad i_n \geq -3°)$$

Secondary flow loss

$$Y_s = 2f(\delta_1/C)b\cos^3\beta_2(\text{tg}\beta_1 - \text{tg}\beta_2)^2 \cdot \sqrt{4 + (\text{tg}\beta_1 + \text{tg}\beta_2)^2}/(h\cos\beta_1)$$

Dunham and Came suggested that $f(\delta_1/C) \approx 0.0334$
can be adopted to account for the boundary layer effect at the
end walls.

Leakage loss $\quad Y_l = 2B\delta_k \cos^3\beta_2(\text{tg}\beta_1 - \text{tg}\beta_2)^2 \cdot \sqrt{4 + (\text{tg}\beta_1 + \text{tg}\beta_2)^2}/h$.

The coefficient of stagnation pressure loss of the guide
blade $\quad \sigma_N = 1/\{1 + (Y_p + Y_s + Y_l)[1 - (1 + (\kappa - 1)M_1^2/2)^{\frac{\kappa}{1-\kappa}}]\}$

20

The efficiency of the rotor blade

$$\eta_r = (H_2 - H_3)/\{H_2 - H_3[1 + (Y_p + Y_s + Y_k) \cdot$$
$$[1 - (1 + (\kappa - 1)M_{w_3}^2/2)^{\frac{\kappa}{1-\kappa}}]]^{\frac{1-\kappa}{\kappa}}\}$$

Entropy increase of the guiding and rotor blades:

$$\Delta s_N = -R\ln\sigma_N \quad \Delta s_R = [\kappa/(1-\kappa)] \cdot R\ln\{[H_2 + \eta_T(V_{\theta_1}u_3 - V_{\theta_1}u_2)/J]/$$
$$[H_2 + (V_{\theta_1}u_3 - V_{\theta_1}u_2)/J]\}$$

To obtain the parameters for which the losses are taken into account, the following set of simultaneous equations must be solved.

Continuity equation upstream of the throat

$$G = [1 + (\kappa - 1)M_n^2/2]^{\frac{1+\kappa}{2(1-\kappa)}} M_n \cdot C_1 e^{-\Delta s_n}$$

Continuity equation downstream of the throat

$$F_n/(F_2\cos\beta_2) = \{[1 + (\kappa - 1)M_n^2/2]/[1 + (\kappa - 1)M_2^2/2]\}^{\frac{\kappa+1}{2(\kappa-1)}}(M_2/M_n)e^{-\Delta s_{nt}}$$

Critical condition of the flow rate $\quad dG/dM_n = 0$

Momentum equation

$$e^{-\Delta s_n(l-l_n)/l}[1 + (\kappa - 1)M_2^2/2]^{\frac{\kappa}{1-\kappa}}(F_2/F_n)$$
$$\cos\beta_n = [1 + (\kappa - 1)M_n^2/2]^{\frac{\kappa}{1-\kappa}} + (\kappa g_c M_n)[1 + (\kappa - 1)M_n^2/2]^{\frac{\kappa}{1-\kappa}}$$
$$\cdot [M_n - M_2\sqrt{1 + (\kappa - 1)M_n^2/2}\cos(\beta_2 - \beta_n)/\sqrt{1 + (\kappa - 1)M_2^2/2}]$$

Expression for loss

$$\Delta s_n = (l_n/l)R\ln\{1 + (Y_p + Y_s + Y_k) \cdot$$
$$[1 - (1 + (\kappa - 1)M_2^2/2)^{\frac{1}{1-\kappa}}]\}$$

For the supercritical condition, another set of simultaneous equations must be used. For the triangular region at the tail (see Figure 2), the following equations can be given:

Continuity equation

$$F_n/(F_2\cos\beta_2) = \{[1 + (\kappa - 1)M_n^2/2]/$$
$$[1 + (\kappa - 1)M_2^2/2]\}^{\frac{\kappa+1}{2(\kappa-1)}}(M_2/M_n)e^{-\Delta s_{nt}}$$

21
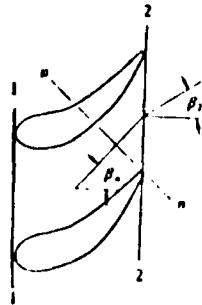
Figure 2. Triangular region at the tail of the turbine
cascade.

Momentum equation

$$(p_2^0/p_n^0)[1 + (\kappa - 1)M_2^2/2]^{\frac{\kappa}{1-\kappa}}(F_2/F_n)\cos\beta_n$$

$$= [1 + (\kappa - 1)M_n^2/2]^{\frac{\kappa}{1-\kappa}}$$

$$+ \kappa g_c M_n[1 + (\kappa - 1)M_n^2/2]^{\frac{\kappa}{1-\kappa}}[M_n - M_2 \cdot$$

Thermodynamic relation

$$\cdot \sqrt{1 + (\kappa - 1)M_2^2/2}\cos(\beta_2 - \beta_n)/\sqrt{1 + (\kappa - 1)M_2^2/2}\,]$$

$$e^{-\Delta s_{n_i}} = p_2^0/p_n^0$$

For the supercritical case, this should be satisfied:

$$\Delta s_n = \Delta s_{ni}$$

Combined with the simultaneous equations derived earlier,
(except the subcritical losses and the expression for the
subcritical exit flow angle), these equations can be solved
to obtain the flow field solution under supercritical condi-
tions. During the solution process, the nonsynchronism of
different parameters may lead to false choking. Hence the
synchronized iterative method is used in this paper to avoid
the occurrence of false choking. In the program, the simul-
taneous equations are first discretized, and then converted
into the finite difference forms at the defined mesh points.
The relaxed iteration method is employed to solve this set of
equations and the flow parameters at different intervals are
obtained, ensuring the synchronism of different parameters
during the computation. The newest streamline pattern and the
corresponding enthalpy and entropy are further obtained, and
the simultaneous equations are solved again. This iteration
process is repeated until a certain degree of accuracy of the

streamline position is satisfied. Since the coefficients of losses and exit flow angle do not have to be given for each design condition in this calculation process, it is possible to conduct the computations for different off-design conditions continuously. Hence the computing efficiency is greatly increased.

III. CALCULATED RESULTS AND ANALYSIS

Based on the set of simultaneous equations, a program is developed and is applied to the calculation of tens of examples and design cases. Fairly satisfactory results are obtained. The convergence speed of the calculation is fast. Only a few iterations of the streamlines are sufficient to reach a 1/1000 accuracy for the relative location of the streamlines. The results obtained from the supercritical calculation are also reasonable, and are found to be in agreement with the experimental results.

Calculations are conducted for the turbine of the 250 kw gas engine developed partly by the Institute of Mechanics, and the turbine of the foreign JT3D-3B engine. The results are satisfactory, as described below:

1. Calculated results for the 250kw turbine

This is a two-stage turbine, designed according to constant operating conditions along the blade span. The blade profile is one of the commonly used airfoil profiles. Single-stage gas turbine tests have been conducted for the first stage, and the second stage separately. Experimental data on the second stage are more complete. Hence the experimental results, and the calculated results of the second stage are compared here.

The flow channel in the 250kw turbine is shown in Figure
3. Figure 4 shows the relation of the expansion ratio π_T
and the reduced flow rate $G\sqrt{T^\circ}/p^\circ$ for the entire off-design
range of the test. The solid line in the figure indicates
the calculated result obtained by the present method, while
the circles indicate the experimental results. It is apparent
that the calculated results agree well with the experimental
results. The error is within 1%.
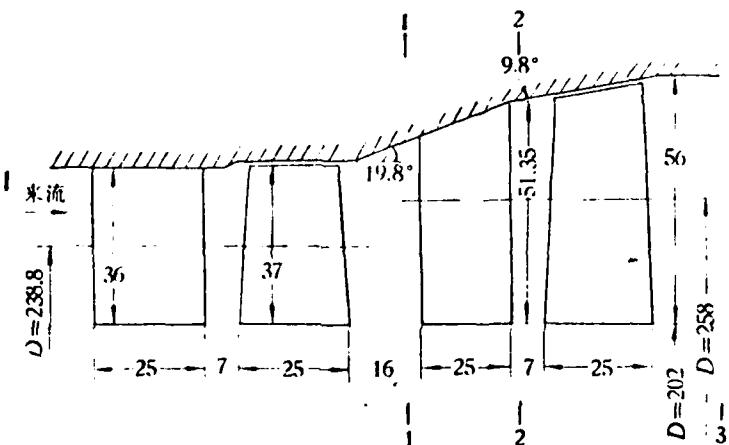
Figure 3.   Flow channel in the 250kw turbine.
            1 - air flow

From Figure 4, it can also be observed that close to the
choking condition, both the experimental data and the theoreti-
cal results from the calculation approach a horizontal line
(that is, the limit of the choking flow rate) with good con-
sistency. The relation between the turbine efficiency n_T
and the expansion ratio π_T is shown in Figure 5. It is obvious
that the calculated results are close to the experimental
results for the entire test range. The error is only about
1%. Figures 6 and 7 compare the distribution of the flow para-
meters in the radial direction. The radial distribution
patterns of the flow angle and the Mach number at the exit plane
of the guiding blade are shown. There is a significant differ-

24

erence between the calculated and experimental results at
certain individual points only. They are fairly consistent
in the mainstream region. The calculated results for the
JT3D-3B are presented in Table 1.
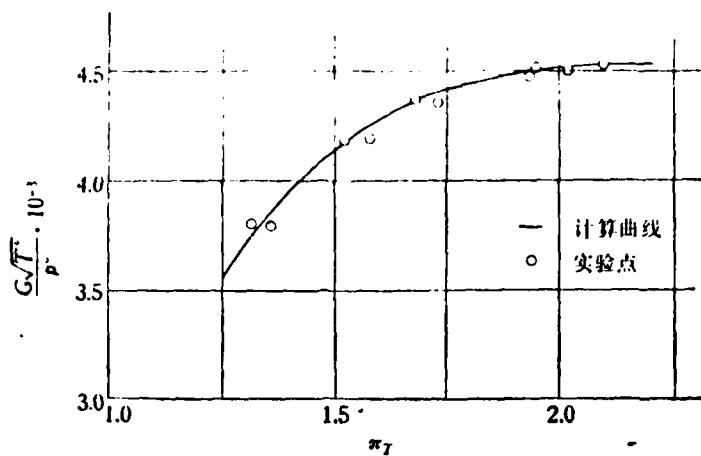
Figure 4.   The relation between $G\dfrac{\sqrt{T^0}}{P^0}$ and π_T of the 250kw-
II stage.
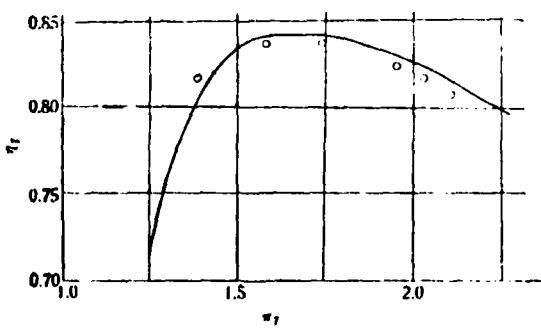
Figure 5.   The relation between n_T and π_T of the 250kw-II
stage.
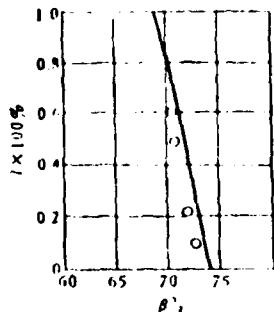
Figure 6. Radial distribution bution of β_2.
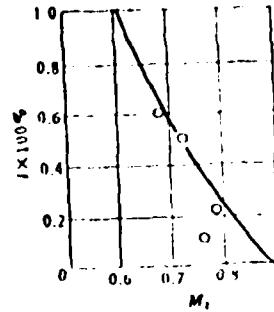
Figure 7. Radial distribution bution of M_2.

Table 1. Comparison of the parameters and calculated results of the JT3D-3B high pressure turbine

Item	Given Parameters	Calculated Result
stagnation pressure at inlet P_1^o	13.182 kg/cm^3	13.182 kg/cm^3
stagnation temperature at inlet T_1^o	1160.6 K	1160.6 K
intake mass flow rate G	88.335 kg/sec	88.01 kg/sec
rotational speed η	9800 rpm	9800 rpm
stagnation pressure at exit P_3^o	6.151 kg/cm^2	6.086 kg/cm^2
stagnation temperature at exit T_3^o	984.9 K	982.7 K
expansion ratio π_T	2.143	2.166
stagnation temperature ratio θ	1.178	1.181

We can now conclude the following:

(1) This method is suitable for calculating the direct

26

problem of transonic turbines at both the design point and the off-design condition. The losses and the exit flow angles can be obtained. The choking flow condition can also be calculated. There is no difficulty in solving the flow parameters for the critical and supercritical cases.

(2) The losses of common blade profiles (e.g. the blade profile of the 250 kw and JT3D-3B turbines) calculated by this method are comparatively reasonable. A comparison between the calculated and the experimental result for the entire test range shows a very satisfactory consistency.

(3) The agreement between the experimental results and the calculated variation of reduced flow rate versus expansion ratio close to the choking conditions indicates that relatively reasonable results can be obtained for the throat choking flow rate by using the critical and supercritical conditions with losses taken into account.

(4) The simultaneous equations including the expression for losses and exit flow angle are applied in this paper to solve for the flow parameters of the turbine. Hence the flow parameters, losses, and exit flow angles can be obtained at the same time. This approach enables us to find a reasonable choking condition quite easily. It also makes the continuous computation for off-design conditions possible.

(5) The consistency of the experimental and the calculated results of the relation between the reduced flow rate and the expansion ratio suggests that the computation method is appropriate for the exit flow angle of common blade profiles within the test range. This conclusion can be observed from Figure 6. The exit flow angle along the blade height is also consistent.

(6) Certain assumptions are made in this method. That is why the limiting Mach number is restricted by the limiting design conditions of the turbine. The error will increase if the Mach number overshoots the limit. Simplifications are also made for the boundary layer loss at the end walls. Hence there is a significant error of the flow parameters near the end walls. This phenomenon requires further investigation.

SYMBOLS

A empirical coefficient

B empirical coefficient

b chord length

C constant or blade thickness

e radius of curvature of the tail of the blade back

F area

G flow rate

H absolute stagnation enthalpy

h blade height or static enthalpy

I relative stagnation enthalpy

l length of the central streamline of the channel between blades

T temperature

t time or distance between blades

u circumferential velocity

V absolute velocity

W relative velocity

Y loss coefficient

α profile angle of the guide blade

β profile angle of the rotor blade or the flow angle of the guide blade

ρ density

i angle of attack

σ recovery coefficient of stagnation pressure

η efficiency

ω angular velocity

δ_κ gap at the tip of the blade

Subscripts:

1 guide blade input

2 guide blade exit

3 rotor blade exit

k leakage

N guide blade

n throat or reduced quantity

nt from the throat to the exit

ne critical

θ tangential

p blade profile

r radial

R rotor blade

s secondary

T turbine

W relative

z axial

Superscripts:

o stagnation state

o' relative stagnation state

29

REFERENCES

[1] Wu. C. H: Application of Radial-Equilibrium Condition to Axial-Flow Compressor and Turbine Design. NACA Rep. 955 (1950).

[2] Wu. C. H: A General Theory of Three-Dimensional Flow in Subsonic and Supersonic Turbomachines of Axial, Radial and Mixed-Flow Types. ASME Paper No. 50-A-79, 1950; Trans ASME Nov. 1952, or NACA TN 2604 (1952).

[3] 中国科学院动力内燃机代表团: 关于简化"径向平衡""轴对称"流动、通流计算、S_1 和 S_2 相对流面三维理论及计算机程序,中国科技情报所, 1974. 10.

[4] Ainley D. G. & G. C. R. Mathieson: A Method of Performance Estimation for Axial Flow Turbines. A. R. C. R&M 2974 (1957).

[5] Vinh-Hai Ngo & D. A. J. Millar: The Design and Performance Prediction of Axial Flow Turbines. Department of Mechanical and Aeronautical Engineering Report, No. ME, 73-3 June, 1973.

[6] 葛满初: 708 高轮变工况监导报告, 1977. 12.

[7] 250 涡轮气轮机通平级动态试验总结之一(气动部分) 1968. 3.

[8] M. E. 杰依奇: 工程气体动力学,电力工业出版社, 1953.

Abstract

We obtain a group of simultaneous equations including equations of S_2 stream surface, simplified S_1 stream surface (for use in the solution of the triangle region at tail of cascade), flow loss and deviation angle correlations for calculation of direct problem in turbomachine. By the solution of these equations, the design point as well as off-design point performances can be calculated.

The essential difference in treating sub-critical, critical and super-critical flow condition is considered. Influence of losses is taken into account in the calculation of choking conditions. We adopt a unified approach to solve these equations. Losses, deviation angles and other flow parameters are obtained in the same iterative process, so that false choking condition will not occur and convergence will be rapid. Computer programm was then completed and may be used in the calculation of the off-design performance of transonic turbines.

In applying this programm to the calculation of the performance of exist turbine stage, we have got satisfactory results. The reduced flow rate, efficiency and expansion ratio are fairly consistent with the experimental results. The difference between the computing results and experimental data is within 1%.

DISTRIBUTION LIST

DISTRIBUTION DIRECT TO RECIPIENT

ORGANIZATION   MICROFICHE

A205 DMATIC   1
A210 DMAAC   1
B344 DIA/RTS-2C   9
C043 USAMIIA   1
C500 TRADOC   1
C509 BALLISTIC RES LAB   1
C510 R&T LABS/AVRADCOM   1
C513 ARRADCOM   1
C535 AVRADCOM/TSARCOM   1
C539 TRASANA   1
C591 FSTC   4
C619 MIA REDSTONE   1
D008 NISC   1
E053 HQ USAF/INET   1
E403 AFSC/INA   1
E404 AEDC/DOF   1
E408 AFWL   1
E410 AD/IND   1
E429 SD/IND   1
P005 DOE/ISA/DDI   1
P050 CIA/OCR/ADD/SD   2
AFIT/LDE   1
FTD
  CCN   1
  NIA/PHS   1
  NIIS   2
LLNL/Code L-389   1
NASA/NST-44   1
NSA/1213/TDL   2

END

DATE
FILMED

10-81

DTIC